Peer-reviewed version available at Sensors 2018; doi:10.3390/s18124208

Article

Design and Implementation of Respiration Rate Measurement System Using Information Filter on Embedded Device

Radius Bhayu Prasetiyo [1], Kyu-Sang Choi [2] and Gi-Hun Yang [3,†*]

[1] University of Science and Technology, South Korea / Korea Institute of Industrial Technology; jq_rbp@yahoo.com
[2] Manufacturing System Group, Korea Institute of Industrial Technology; kschoi@kitech.re.kr
[3] Robotics Group, Korea Institute of Industrial Technology; yanggh@kitech.re.kr
* Correspondence: yanggh@kitech.re.kr; Tel.: +82-031-8040-6389
† Current address: Korea Institute of Industrial Technology (KITECH) A-#335, 143 Hanggaulro, Sangnok-gu, Ansan-si, Gyeonggi-do, 426-910, South Korea

Version August 8, 2018 submitted to Preprints

Abstract: In this work, an algorithm was developed to measure the respiration rate for an embedded device that can be used by a field robot for relief operation. With this algorithm, the rate measurement was calculated based on direct influences of respiratory-induced intensity variation (RIIV) on blood flow in cardiovascular pathways. For that, a photoplethysmogram (PPG) sensor was used to determine changes in heartbeat frequencies. The PPG sensor readings were filtered using an Information Filter and a Fast Fourier transform (FFT) to determine the state of RIIV. With a relatively light initialization, the information filter can estimate unknown variables based on a series of measurements containing noise and other inaccuracies. Therefore, this filter is suitable for application on an embedded device. For faster calculation time in the implementation, the FFT analysis was calculated only for a major peak in the frequency domain. Test and measurement of respiration rate was conducted based on the device algorithm and spirometer. Heartbeat measurement was also evaluated by comparing the heartbeat data of the PPG sensor and the medical tool kit. Based on the test, the implemented algorithm can measure respiration rate with about 80% accuracy compared with the spirometer.

Keywords: Photoplethysmography (PPG), respiration rate, information filter

1. Introduction

In recent years, rapid technological advances have led to great developments in the field of robotics, especially for medical purposes [1]. From a microscopic scale to a large robotic surgery system, these developments bring significant progress in treatment and the health-care system [2–5]. The robot is also getting more portable and compact as it is needed for assessing first aid in a dangerous environment that cannot be accessed by personal medical help [6–13]. Furthermore, the robot needs to be able to locate and preliminarily determine the physical state of an injured person so that a correct course of treatment can be quickly performed by the medical help. Therefore, a medical sensory system that can determine the physical state must be implemented in the robotic system, especially that which is related to vital health conditions, such as heartbeat and respiration rate.

Respiration rate is a vital biosignal state that determines the physical state of the pulmonary system, which directly influences blood flow in cardiovascular pathways. Because of that, the measurement of blood flow in cardiovascular pathways can reflect a heartbeat condition as inhale and exhale activities can directly increase or decrease blood flow in those pathways [14–17]. Therefore, by measuring the changes of blood flow or heartbeat frequencies in the cardiovascular stream, the respiration rate can also be determined. The parameter of respiratory-induced intensity variation (RIIV) can also be analyzed based on those changes [15–22].

Photoplethysmography (PPG) is a method that uses an optical measurement to detect blood volume changes in the body caused by the cardiovascular system [14–22]. The PPG measurement can be achieved by employing a light source and a photodetector. Red or near-IR light-emitting diode (LED) with a wavelength of more than 600 nm is commonly used as the light source for the PPG sensor. This LED works as a transmitter that will illuminate the skin tissue and will be captured by the photodetector. The variations of light intensity in the skin detected by the photodetector can be associated with changes in blood volume in the captured area. Therefore, using such noninvasive method, the PPG sensor can be used to measure the blood flow rate caused by the cardiovascular system that reflects the heartbeat condition.

In this work, an algorithm for measuring the respiration rate was developed for an embedded device. A field robot for relief operation will be equipped with the device and will be deployed for search and rescue operations. Additionally, to be able to provide first aid in a critical situation, the robot will also carry other medical instruments, such as syringe and oxygen delivery system. Furthermore, the robot must be able to locate the victims and preliminarily determine their physiological state, such as their heartbeat, respiration rate, and body temperature. For that, the robot will deploy the embedded device from a safe compartment after removing obstruction in measurement area. Therefore, the device must be small, lightweight, and low powered. Likewise, the algorithm should not be too complicated and can be run in such limited resources with reasonable reliability. Here, the algorithm was simplified so that it can be implemented to an embedded device with dimension of about $50 \times 40 \times 30$ mm and a weight of about 40 grams.

2. Respiration Rate Measurement Algorithm

The algorithm for respiration rate measurement was derived from raw data readings of the PPG sensor. The raw data then filtered using information filter to remove noises in the heartbeat signal readings. Information filter or inverse covariance filter, is a well known filter that has same function and procedures as Kalman Filter [23]. With a relatively light initialization, the information filter can estimate unknown variables based on a series of measurements containing noise and other inaccuracies. Therefore, this filter can produce optimal parameters estimation of state and observation model from measurements with Gaussian noise, such as object tracking system [23–25].

Same as Kalman Filter, the information filter procedure consists from initialization, propagation, and update [23]. Based on this, the filter's algorithm can be derived from those three approaches. In here, information filter will take signal from PPG sensor as measurement input and track its value a_k and rate of change b_k from time $k-1$ to time k ($T_{k|k-1}$) as shown in equation 1.

$$\begin{bmatrix} a_k \\ b_k \end{bmatrix} = F \begin{bmatrix} x_{k-1} \\ v_{k-1} \end{bmatrix} \tag{1}$$

where:

$$F = \begin{bmatrix} 1 & T_{k|k-1} \\ 0 & 1 \end{bmatrix} \tag{2}$$

During initialization, the information filter sets its state ($\hat{y}_{0|0}$) and covariance ($P^{-1}_{0|0}$) to zero. This shows that information filter has very light initialization compared with kalman filter which needs large number for its covariance to cover all input data during initialization time. Then the filter will propagate the state and covariance by using equation 3 and 4. In here, I is an identity matrix 2x2 and Q is calculated based on equation 7 with $qdef$ equals to 0.375.

$$\hat{y}_{k|k-1} = (I + AQ)^{-1} F^{-T} Y_{k-1|k-1} \tag{3}$$

$$P^{-1}_{k|k-1} = (I + AQ)^{-1} A \tag{4}$$

where:

$$I = I_2 \tag{5}$$

$$A = F^{-T} P_{k-1|k-1}^{-1} F^{-1} \tag{6}$$

$$Q = qdef \begin{bmatrix} \frac{T_{k|k-1}^4}{3} & \frac{T_{k|k-1}^4}{3} \\ \frac{T_{k|k-1}^4}{3} & T_{k|k-1}^2 \end{bmatrix} \tag{7}$$

$$qdef = 0.375 \tag{8}$$

When PPG sensor captures a heartbeat signal at time k, the information filter will update its propagated state and covariance by using equation 9 and 10. In this update, value of matix H and R is configured to reduce noise and avoid non-linearity from PPG signal value.

$$\hat{y}_{k|k} = \hat{y}_{k|k-1} + H^T R^{-1} zk \tag{9}$$

$$P_{k|k}^{-1} = P_{k|k-1}^{-1} + H^T R^{-1} H \tag{10}$$

where:

$$H = \begin{bmatrix} 1 & 0 \\ 0 & 0 \end{bmatrix} \tag{11}$$

$$R = \begin{bmatrix} 50 & 50 \\ 50 & 50 \end{bmatrix} \tag{12}$$

Finally, equation 13 can generate output of the information filter based on the updated state and covariance (i.e. $\hat{x}_{k|k}$). In here, the filter output is a representative of variables in equation 1.

$$\hat{y}_{k|k} = P_{k|k}^{-1} \hat{x}_{k|k} \tag{13}$$

After filtered, the changes in heartbeat signal frequencies were analyzed using an Fast Fourier transform (FFT) to get the RIIV distribution. The distribution was basically accumulated from a buffered FFT output in about a 20-second interval. Additionally, the distribution was updated every data sampling period. Finally, based on a peak-to-peak detection on the RIIV distribution, the respiration rate was calculated for each second.

3. Implementation of Algorithm on Embedded Device

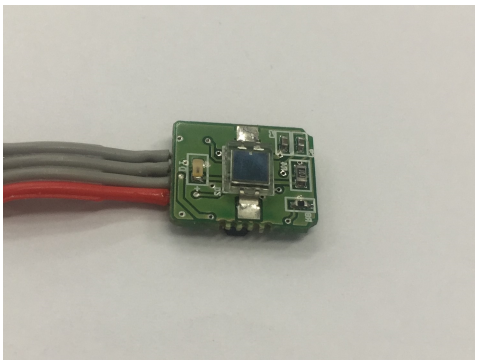

Figure 1. PPG Sensor Board, Laxtha RP520.

The embedded device consists of a PPG sensor, as shown in Figure 1, for heartbeat measurement, a thermometer sensor to facilitate body temperature measurement, and a CPU of an ARM processor,

Preprints (www.preprints.org) | NOT PEER-REVIEWED | Posted: 8 August 2018 doi:10.20944/preprints201808.0161.v1

Peer-reviewed version available at Sensors 2018; doi:10.3390/s18124208

as shown in Figure 2. A Teensy 3.2 board was chosen as a base for the hardware development of the embedded device as the board has a small footprint with a 13-bit usable ADC and an ARM Cortex-M4 processor. The system can be used with a low-powered battery of 3.3 V with a CPU speed of 72 MHz. Using this system, the algorithm results can also be logged to other devices via serial communication.

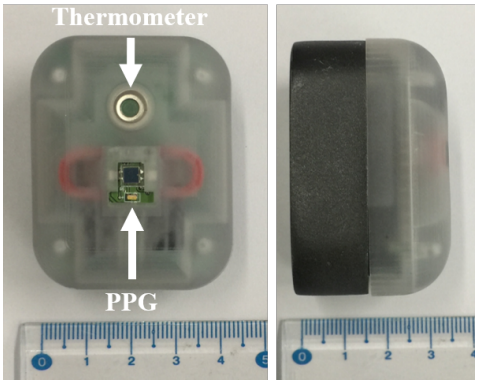

Figure 2. The Embedded Device for Respiration Rate Measurement.

The heartbeat signal from the PPG sensor in the embedded device was captured in a form of discrete number with noises via a 13-bit ADC system. Because the computational speed of the embedded device is relatively slow compared to a high-end computer system, the algorithm of the respiration rate measurement must be simplified so that it can be used in such a limited system.

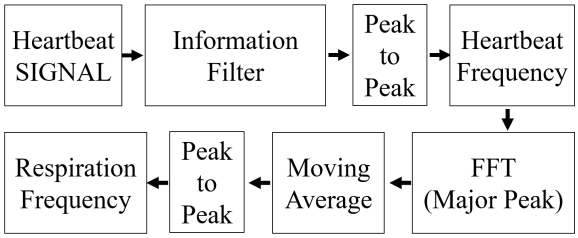

Figure 3. Simplified Algorithm on The Embedded Device.

As shown in Figure 3, the heartbeat signal in the embedded device that was captured from a 13-bit ADC system and contains measurement noises, was approached using an information filter. With this approach, the discrete numbers of ADC reading can be linearized and the noises can also be reduced so that it can be observed more effectively.

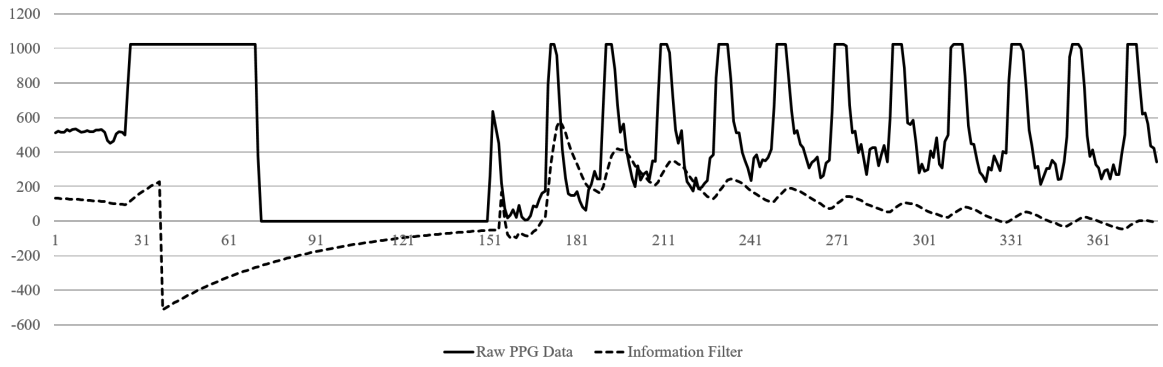

Figure 4. Typical Signal Filtering.

Fig. 4 illustrates typical output signal of the information filter. In this figure, raw data from ADC system were displayed as a solid line and the filter output were distributed in a dotted line in every time step of about 50 ms. As shown in the figure, the PPG sensor took about 140 time step (7 seconds) before it started measuring the heartbeat signal. During this time, the ADC output was raised to a maximum value and then significantly dropped non-linearly to zero. On the other hand, the information filter output can follow linearly the ADC data on every time step with delay of about 3 time step or about 150 ms. Based on the figure, initial heartbeat detection will be calculated on time step 180 which has a delay of about 30 time step or about 1.5 seconds from the first detected heartbeat signal from PPG sensor. This means that the algorithm has about 1.5 seconds of delay or initial detection time for heartbeat measurement.

Once filtered, the frequencies of the heartbeat signal were analyzed using an FFT. In the embedded device, the analysis on the FFT was conducted on a major peak only and directly measured on the frequency domain. Because the FFT output can actually describe the changes in the input signal, changes of intensity in heartbeat signal due to intrathoracic pressure can also be measured by monitoring the major peak's variation. Then with a moving average filter and peak-to-peak detection, the respiration rate can be calculated based on these variations that show the changes on the filtered heartbeat signal [15,16,22,26]. In here, the FFT analysis was configured with 64 data points and frequency resolution of 40 Hz. Additionally, the moving average filter was calculated based on 20 samples of FFT output with sampling time of 50 ms.

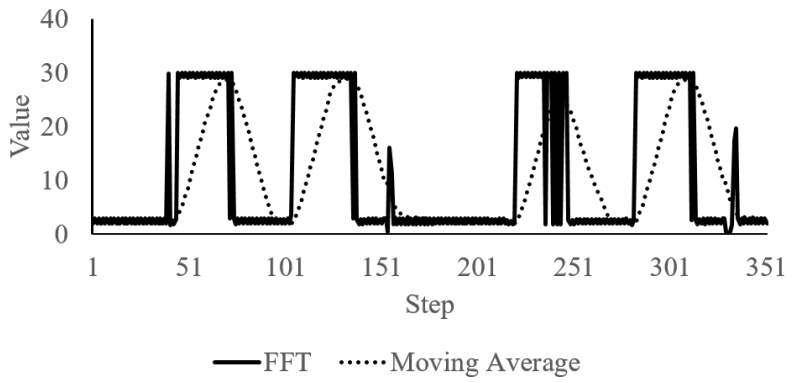

Figure 5. FFT and Moving Average Signal.

Figure 5 shows FFT analysis and moving average filter output. The solid line illustrates the major peak's distribution in each time step. On the other hand, moving average output that were calculated based on the major peak values, were distributed as a dotted line. As shown in the figure, when the major peak intensity is changed, the moving average value will follow it linearly in a form of a signal peak. Therefore, in this figure, there are about four significant changes in about 300 time step which can be calculated as a respiration rate of about 0.27 Hz.

During implementation in the embedded device, the filter optimization was also tested with induced-stress measurement of a test subject sitting on a chair after exercising. The exercise was performed by running on a treadmill with inclination level of 2% and speed level of 5 for about 5 minutes. While the subject was still in recovery phase or post-exercise, measurement of heartbeat and respiration rate was immediately conducted for about 120 seconds.

4. Experiment and Results

In the case of heartbeat frequency calculation, a pulse oximeter was used to measure the heartbeat frequency of the test subject, as shown in Figure 6. In here, measurement outputs from the oximeter and embedded device were logged simultaneously during the test.

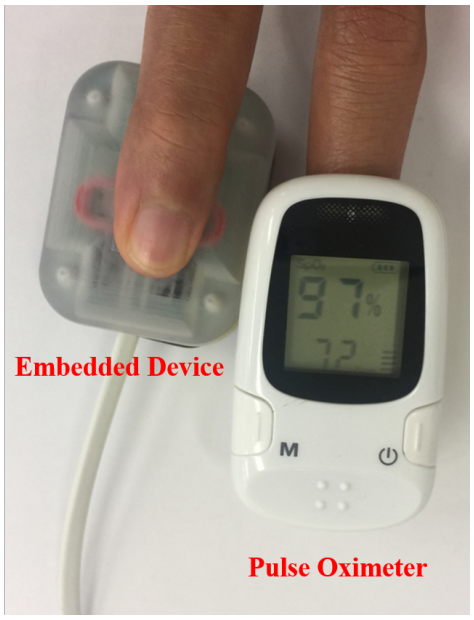

Figure 6. Test Setup with Subject's Hand.

On the other hand, a spirometer (i.e., Vernier Spirometer with order code SPR-BTA) was utilized to validate the respiration rate algorithm results, as shown in Figure 7. Here, the test subject held the spirometer in one hand and breath through it while the other hand was put on the embedded device and pulse oximeter, as shown in Figure 8. The spirometer was connected to Vernier SensorDAQ that can send the spirometer signal data to a computer or PC. During the test, the embedded device was also connected to main PC via serial communication for data logging only. All computation and algorithm process was conducted in embedded device. Data from the embedded device, spirometer, and pulse oximeter then logged to a file using LabView interface.

Figure 7. Vernier Spirometer.

Preprints (www.preprints.org) | NOT PEER-REVIEWED | Posted: 8 August 2018 doi:10.20944/preprints201808.0161.v1

Peer-reviewed version available at Sensors 2018; doi:10.3390/s18124208

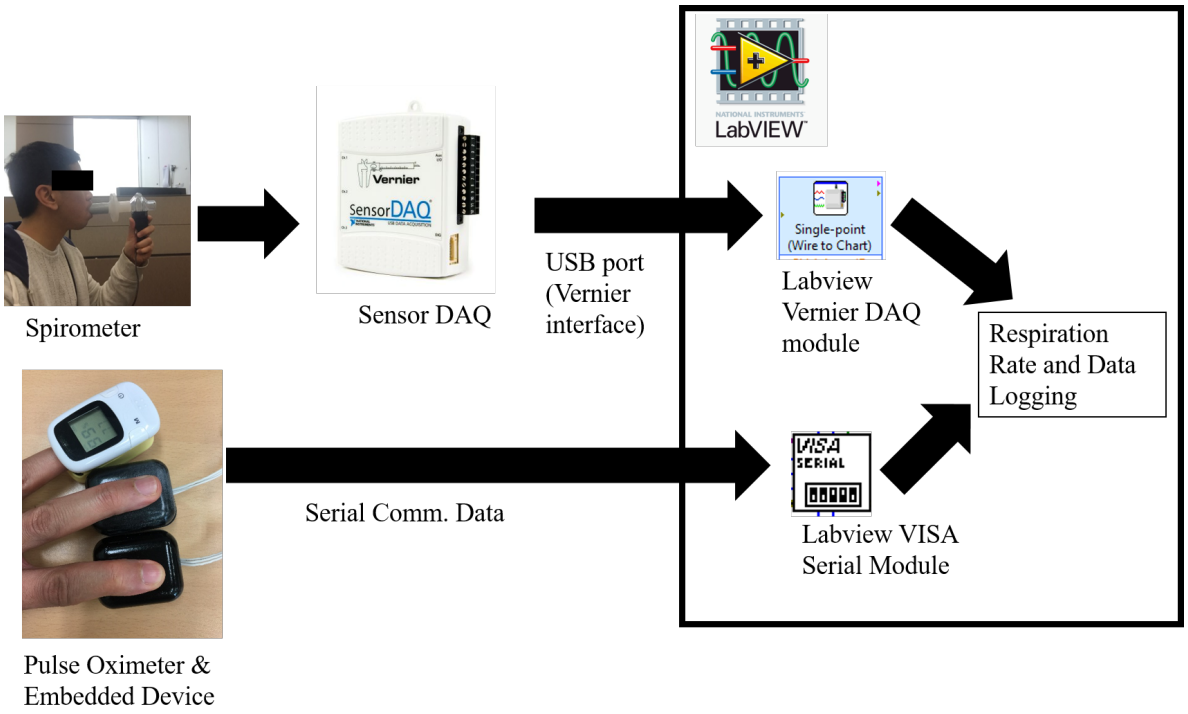

Figure 8. Experiment Setup

This experiment has ten test subjects who have an average age of 30 years and are in a healthy condition. For each subject, about 10 measurements was performed with one measurement time of about 5-10 minutes for normal relaxed breathing and about 120 seconds for the post-exercise measurement. Between measurements, there was a 60-second time interval for resetting and stabilizing the measurement values of the oximeter and the embedded device. During this time interval, the oximeter and the embedded device were detached and reattached to the test subject's finger. Then the differences between the algorithm results with the pulse oximeter and spirometer output were calculated to validate the heartbeat and the respiration rate measurement.

The measurement results of the embedded algorithm was evaluated on two breathing conditions (i.e., normal relaxed and post-exercise) using pulse oximeter and spirometer. Based on these, performance of the embedded algorithm, especially that for respiration measurement, was calculated for the two conditions.

Table 1. Comparison of Heartbeat (bpm) Measurement between Pulse Oximeter and Embedded Algorithm.

Method / Tool	Min	Average	Max
Pulse Oximeter	58	77	84
Embedded Algorithm	57	79	89

Table 2. Comparison of Respiration Rate (Hz) Measurement between Spirometer and Embedded Algorithm.

Method / Tool	Min	Average	Max
Spirometer	0.22	0.29	0.36
Embedded Algorithm	0.24	0.26	0.30

Preprints (www.preprints.org) | NOT PEER-REVIEWED | Posted: 8 August 2018 doi:10.20944/preprints201808.0161.v1

Peer-reviewed version available at Sensors 2018; doi:10.3390/s18124208

On the other hand, the heartbeat measured by the algorithm in the embedded device was averaged at 79 bpm as shown in Table 1. Based on the table, the heartbeat measurement value was similar to that of a pulse oximeter with a maximum difference of 5 bpm. In Table 2, the respiration rate was measured from 0.24 Hz to 0.30 Hz based on the embedded algorithm with a difference of 0.03 Hz on the average value.

Table 3. Differences of The Algorithm in Embedded Device.

Parameter	Min	Average	Max
Heartbeat Rate Diff. (%)	0.03	4.31	8.07
Respiration Rate Diff. (%)	0.43	8.12	18.8

Table 3 shows measurement differences of the embedded device on the test subject during normal relaxed breathing and post-exercise. Here, the heartbeat rate difference is about 4.31% compared with that of a pulse oximeter output. On the other hand, the respiration rate difference is averaged at 8.12% compared with spirometer results. This result shows that the simplification procedures and filtering process of the raw heartbeat signal are successfully implemented in the embedded device with reasonable average accuracies of about 90%.

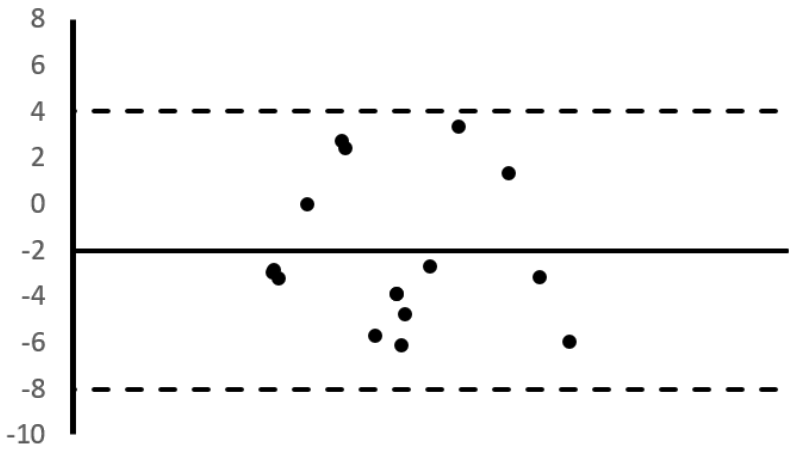

Figure 9. Bland-Altman Plot of Heartbeat Rate Differences (bpm)

Figure 9 illustrate these differences of heartbeat rate measurement result of the embedded device compared with that of pulse oximeter output. Table 4 shows the plot parameter of heartbeat rate differences. The figure and table describe a bias of -2.03 bpm, with lower limits of agreement of -8.06 bpm and upper limits of agreement of 4 bpm. With that, the average of the difference is about 4.31% with standard deviation of about 3.17.

Table 4. Parameter Values of Heartbeat Rate Differences (bpm)

Parameter	Value
Bias	-2.03
Standard Deviation	3.17
Upper Bound	4.00
Lower Bound	-8.06

Likewise, Figure 10 display differences of respiration rate measurement result of embedded algorithm compared with spirometer on the two breathing conditions. As shown in

Table reftable:barespparam, the bias is about 0.01 Hz with lower and upper limits of agreement of -0.03 Hz and 0.06 Hz respectively. Additionally, the average differences is about 8% with standard deviation of about 0.02.

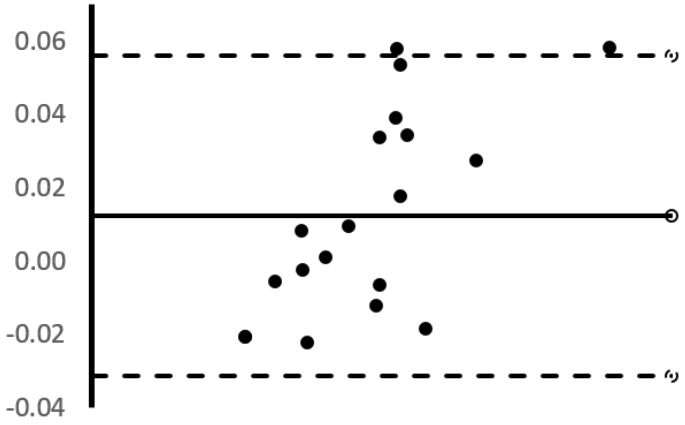

Figure 10. Bland-Altman Plot of Respiration Rate Differences (Hz)

Table 5. Parameter Values of Heartbeat Rate Differences (bpm)

Parameter	Value
Bias	0.01
Standard Deviation	0.02
Upper Bound	0.06
Lower Bound	-0.03

In addition to a validation test, the initial detection and settling time of the algorithm in the embedded device was also calculated. Here, the distribution was calculated to observe the computational time of the algorithm implementation in the embedded device. The initial detection time was calculated between the first PPG signal detection and the first heartbeat and respiration rate calculation output.

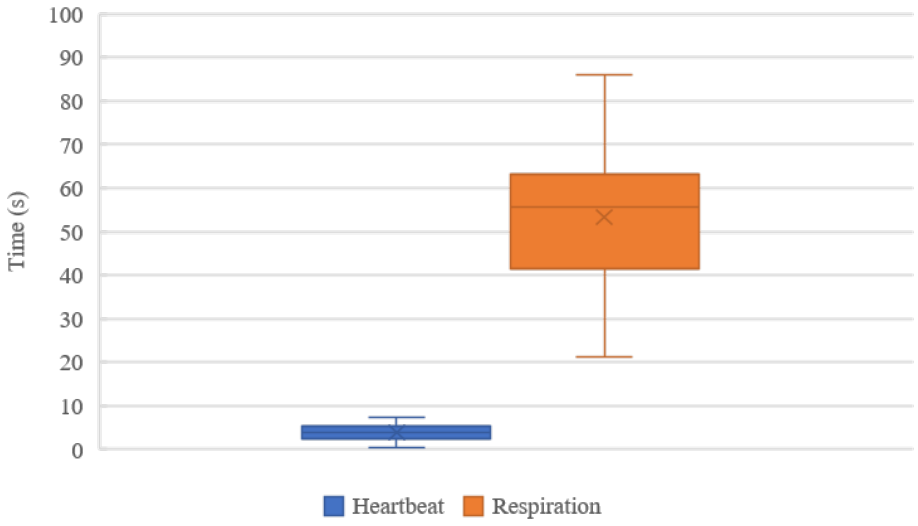

Figure 11. Heartbeat and Respiration Initial Time Distribution.

Figs. 11 shows the average distribution of heartbeat and respiration measurement initial time of the embedded algorithm. On this figure, the initial heartbeat detection time is averaged on about 4 seconds with the fastest time is about 0.33 seconds from the first heartbeat signal which is detected by the PPG sensor. On the other hand, the initial respiration detection time is about 53 seconds due to FFT sampling time. With that, respiration rate output values of the algorithm in the embedded device are converged in less than 90 seconds with fastest detection time is about 21 seconds, as shown in Table 6.

Table 6 shows initial detection time and measurement differences of the embedded device. In here, the heartbeat rate difference is about 4.15% compared with that of pulse oximeter output. On the other hand, respiration rate difference is averaged at 8.12% compared with spirometer on normal relaxed and post-exercise breathing conditions.

Table 6. Evaluation Result of The Algorithm in Embedded Device.

Parameter	Min	Average	Max
Initial Heartbeat Detection Time (s)	0.33	3.81	7.43
Initial Respiration Detection Time (s)	21.14	53.32	86.14
Heartbeat Rate Diff. (%)	0.13	4.15	8.87
Respiration Rate Diff. (%)	0.43	8.12	18.8

5. Conclusion

Simplified algorithm to measure respiration rate was successfully implemented to the embedded device. The device utilized a PPG sensor to capture heartbeat signal which then was filtered using information filter. Then FFT analysis was conducted to calculate the respiration rate based on RIIV observation from the filtered data. In here, the algorithm can measure heartbeat and respiration rate with bias of -2.03 bpm and 0.01 Hz respectively. In addition, based on test results of ten subjects with two breathing conditions (i.e. normal and post-exercise breathing), the algorithm computation has standard deviation of 3.17 for the heartbeat measurement and 0.02 for the respiration.

Based on the results, it can be concluded that the algorithm in the embedded device can measure the heartbeat rate with a maximum of about 10% difference or about 90% accuracy. On the other hand, the delay of the computational process is about 4 seconds from the first detected heartbeat signal by PPG sensor, with additional 7 seconds for the sensor initialization. Then, on normal and post-exercise condition, the embedded device can measure the respiration rate with an average difference of about 8% or about 90% accuracy. Additionally, the maximum difference is about 19% (or accuracy of about 80%) compared with the spirometer, which proves the effectiveness of information filter on the embedded device.

6. Future Work

In this current development, the heartbeat and respiration rate measurement was conducted on a conscious person in a stable environment. The algorithm for the embedded device was successfully implemented with a reasonable measurement value compared with other medical devices. For general use and future development, the embedded device will be attached to a manipulator and tested in a different environment. In addition, the measurement and test of the embedded device will be conducted on a varying test condition, such as age and body posture, of an unconscious or sleeping subject. Also, spontaneous and controlled breathing will be observed as it tends to affect the PPG sensor reading, especially that for the RIIV measurements [22].

Acknowledgments: This research was supported by Korea Electronics Technology Institute (KETI) as part of the "development of dependable soft manipulator and multi-function gadgets for relief operation" (ND 170004).

References

1. Khan, M. The Development of a Mobile Medical Robot Using ER1 Technology **2013**. *32*, 34–37.

2. Lee, J.; Kim, E.; Kim, S.; Jeon, S.; Choi, H. A flexible microrobots with magnetic actuation for medical tool **2016**. pp. 184–185.
3. Ishiyama, K.; Sendoh, M.; Arai, K. Magnetic micromachines for medical applications **2002**. *242*, 41–46.
4. Qiu, F.; Nelson, B.J. Magnetic Helical Micro- and Nanorobots: Toward Their Biomedical Applications. *Engineering* **2015**, *1*, 021 – 026. doi:https://doi.org/10.15302/J-ENG-2015005.
5. Bell, D.J.; Leutenegger, S.; Hammar, K.M.; Dong, L.X.; Nelson, B.J. Flagella-like Propulsion for Microrobots Using a Nanocoil and a Rotating Electromagnetic Field. Proceedings 2007 IEEE International Conference on Robotics and Automation, 2007, pp. 1128–1133. doi:10.1109/ROBOT.2007.363136.
6. Phee, S.; C Low, S.; Sun, Z.; Y Ho, K.; M Huang, W.; M Thant, Z. Robotic system for no-scar gastrointestinal surgery **2008**. *4*, 15–22.
7. Barkana, D.E. Design and implementation of a control architecture for robot-assisted orthopaedic surgery. *The International Journal of Medical Robotics and Computer Assisted Surgery* **2010**, *6*, 42–56. doi:10.1002/rcs.287.
8. Tavakoli, M.; Patel, R.V.; Moallem, M. Haptic interaction in robot-assisted endoscopic surgery: a sensorized end-effector. *The International Journal of Medical Robotics and Computer Assisted Surgery* **2005**, *1*, 53–63. doi:10.1002/rcs.16.
9. Wolf, A.; Jaramaz, B.; Lisien, B.; DiGioia, A.M. MBARS: mini bone-attached robotic system for joint arthroplasty. *The International Journal of Medical Robotics and Computer Assisted Surgery* **2005**, *1*, 101–121. doi:10.1002/rcs.20.
10. Kobayashi, Y.; Tomono, Y.; Sekiguchi, Y.; Watanabe, H.; Toyoda, K.; Konishi, K.; Tomikawa, M.; Ieiri, S.; Tanoue, K.; Hashizume, M.; Fujie, M.G. A surgical robot with vision field control for single port endoscopic surgery. *The International Journal of Medical Robotics and Computer Assisted Surgery* **2010**, *6*, 454–464. doi:10.1002/rcs.355.
11. Zamorano, L.; Li, Q.; Jain, S.; Kaur, G. Robotics in neurosurgery: state of the art and future technological challenges. *The International Journal of Medical Robotics and Computer Assisted Surgery* **2004**, *1*, 7–22. doi:10.1002/rcs.2.
12. Kuebler, B.; Seibold, U.; Hirzinger, G. Development of actuated and sensor integrated forceps for minimally invasive robotic surger. *The International Journal of Medical Robotics and Computer Assisted Surgery* **2005**, *1*, 96–107. doi:10.1002/rcs.33.
13. Cepolina, F.; Michelini, R.C. Review of robotic fixtures for minimally invasive surgery. *The International Journal of Medical Robotics and Computer Assisted Surgery* **2004**, *1*, 43–63. doi:10.1002/rcs.5.
14. Nakajima, K.; Tamura, T.; Miike, H. Monitoring of heart and respiratory rates by photoplethysmography using a digital filtering technique. *Medical Engineering & Physics* **1996**, *18*, 365 – 372. doi:https://doi.org/10.1016/1350-4533(95)00066-6.
15. Karlen, W.; Raman, S.; Ansermino, J.M.; Dumont, G.A. Multiparameter Respiratory Rate Estimation From the Photoplethysmogram. *IEEE Transactions on Biomedical Engineering* **2013**, *60*, 1946–1953. doi:10.1109/TBME.2013.2246160.
16. Lovett, P.; M Buchwald, J.; Stürmann, K.; Bijur, P. The Vexatious Vital: neither clinical measurements by nurses nor an electronic monitor provides accurate measurements of respiratory rate in triage **2005**. *45*, 68–76.
17. Yousefi, R.; Nourani, M. Separating Arterial and Venous-Related Components of Photoplethysmographic Signals for Accurate Extraction of Oxygen Saturation and Respiratory Rate. *IEEE Journal of Biomedical and Health Informatics* **2015**, *19*, 848–857. doi:10.1109/JBHI.2014.2334697.
18. Allen, J. Photoplethysmography and its application in clinical physiological measurement. *Physiological Measurement* **2007**, *28*, R1.
19. Sun, B.; Zhang, Z. Photoplethysmography-Based Heart Rate Monitoring Using Asymmetric Least Squares Spectrum Subtraction and Bayesian Decision Theory. *IEEE Sensors Journal* **2015**, *15*, 7161–7168. doi:10.1109/JSEN.2015.2473697.
20. Dyell, D.; Rogowski, C.; Kahler, S.; Milan, J. Real-time monitoring systems and methods in a healthcare environment, 2016. US Patent App. 14/835,709.
21. Zhang, Z. Photoplethysmography-Based Heart Rate Monitoring in Physical Activities via Joint Sparse Spectrum Reconstruction. *IEEE Transactions on Biomedical Engineering* **2015**, *62*, 1902–1910. doi:10.1109/TBME.2015.2406332.

22. Li, J.; Jin, J.; Chen, X.; Sun, W.; Guo, P. Comparison of respiratory-induced variations in photoplethysmographic signals. *Physiological Measurement* **2010**, *31*, 415.
23. Challa, S.; Morelande, M.; Mušicki, D.; Evans, R. *Fundamentals of Object Tracking*; Cambridge books online, Cambridge University Press, 2011.
24. LaViola, J.J. A comparison of unscented and extended Kalman filtering for estimating quaternion motion. Proceedings of the 2003 American Control Conference, 2003., 2003, Vol. 3, pp. 2435–2440 vol.3. doi:10.1109/ACC.2003.1243440.
25. Simmons, L.P.; Welsh, J.S. Unscented Kalman Filter based finger tracking utilising magnetoresistive sensors. 2015 American Control Conference (ACC), 2015, pp. 5128–5133. doi:10.1109/ACC.2015.7172139.
26. Nakajima, K.; Tamura, T.; Ohta, T.; Miike, H.; Oberg, P.A. Photoplethysmographic measurement of heart and respiratory rates using digital filters. Proceedings of the 15th Annual International Conference of the IEEE Engineering in Medicine and Biology Societ, 1993, pp. 1006–1007. doi:10.1109/IEMBS.1993.978978.